Mechanisms for Low-Energy (0.5−30 eV) Electron-Induced Pyrimidine Ring Fragmentation within Thymine- and Halogen-Substituted Single Strands of DNA

ARTICLE *in* THE JOURNAL OF PHYSICAL CHEMISTRY B · JUNE 2000

Impact Factor: 3.3 · DOI: 10.1021/jp9938112

3 AUTHORS, INCLUDING:

H. Abdoul-Carime

Institut National de Physique Nucléaire et de …

101 PUBLICATIONS **2,292** CITATIONS

SEE PROFILE

Mechanisms for Low-Energy (0.5−30 eV) Electron-Induced Pyrimidine Ring Fragmentation within Thymine- and Halogen-Substituted Single Strands of DNA

Pierre-Cyrille Dugal, Hassan Abdoul-Carime, and Léon Sanche*

Groupe du Conseil de Recherches Médicales en Sciences des Radiations, Département de Médecine Nucléaire et de Radiobiologie, Faculté de Médecine, Université de Sherbrooke, Sherbrooke, Québec, Canada, J1H 5N4

Received: October 27, 1999; In Final Form: February 24, 2000

Low-energy (0.5−30 eV) electron irradiation of the thymine- and halogen-substituted nonamers Au/Cy*$_6$T$_3$ and Au/Cy*$_6$(FU,BrU,IU)$_3$, chemisorbed onto a gold surface, leads to the desorption of neutral CN and OCN from fragmentation of the DNA base ring. No neutral halogen-containing species are detected. The cross sections at 15 eV for CN and OCN desorbing from the substituted oligomers bromouracil, fluorouracil, iodoracil, and thymine are measured to be 7.5-, 4.5-, (2.5−3.0)-, and (3.0−3.5) × 10^{-17}cm^2, respectively; the difference between T and BrU is about 2- to 3-fold over the investigated energy range. The decrease of neutral species produced, in the sequence BrU > FU > IU ≈ T, is observed over the entire 0.5−30 eV range. Unimolecular dissociation of resonant and nonresonant electron-induced uracil-like radicals is likely to be responsible for the formation/desorption of these neutral species. Above 20 eV incident electron energy, the initial process essentially involves nonresonant interactions, whereas within the 5−20 eV energy range, core-excited resonances are implicated. At lower energy, the neutral fragments, which are observed only for bromouracil-substituted oligonucleotides, are induced via a shape resonance. The behavior of the magnitude of the CN and OCN yields with incident electron energy, along with empirical threshold calculations for neutral fragment formation and considerations of transient anion dissociation dynamics, led us to propose possible mechanisms for pyrimidine ring fragmentation by slow electron impact.

Introduction

It is well established that the impact of electrons on metallic and dielectric surfaces can fragment or decompose adsorbate molecules.[1−10] The species produced often further react with the neighboring atoms or molecules, or both, leading to the formation of new compounds.[1,3,5,9−11] This electron-induced chemistry is initiated by electronic transitions to dissociative states, which can often be identified by monitoring one or more of the dissociation products leaving the surface.[8,11−13] At low electron energies (0−20 eV), and more particularly below the threshold for dipolar dissociation, dissociative electron attachment (DEA) has been found to contribute to the fragmentation of adsorbates with considerable cross section.[14] In experiments that allowed the measurement of the electron-stimulated desorption (ESD) of stable anions, the contribution from DEA to the decomposition of adsorbates could clearly be identified, and the magnitude of the process could be measured as a function of incident electron energy.[2,8,10,11] Moreover, in experiments[8,10−15] where the final products from slow-electron (0−20 eV)-induced reactions were detected as a function of incident electron energy, it was shown that DEA was involved in the initial fragmentation.

Reactions induced by low-energy electron impact are of interest to diverse fields such as lithography,[6,7,15−17] surface photochemistry,[18] dielectric breakdown,[19] astrophysics,[20,21] and radiation chemistry and biology.[22] In the systems irradiated with high-energy particles, copious amounts of low-energy secondary electrons generated by ionization interact with the medium where they can induce specific reactions. It was calculated that 80% of the secondary electrons produced along the ionization tracks possess energies less than 20 eV and that their population decays exponentially with increasing energy.[23] Despite the predominance of such low-energy electrons in irradiated systems, their action in biologically relevant molecules is still poorly understood, and we presently have no detailed knowledge of the chemistry they can induce. So far, only a few experiments have been performed to probe chemical reactions induced by low-energy electrons on biological molecules; these experiments have been conducted primarily on thin films of DNA bases[24] and oligonucleotides[25,26] which serve as model systems of single-strand DNA damage. In the latter case, ESD was combined with an adsorption technique, similar to that used to prepare self-assembled monolayers (SAMs)[27], to efficiently introduce clean samples of large biomolecules into an ultrahigh vacuum chamber. It has been demonstrated that below 20 eV the impinging electrons dissociate the DNA bases within the oligomers via a resonant interaction such as DEA. Moreover, production of these neutral species depends strongly on the nature of the DNA bases involved. Indeed, a comparative study of damage induced by low-energy 1−30 eV electrons on thymine- (T-) and bromouracil- (BrU-) substituted oligonucleotides[26] shows an enhancement of the neutral fragments production for BrU. Because the main difference between both pyrimidine bases lies on the methyl group in T and the bromine atom at the same position in BrU, a systematic study of halouracils (FU, IU, and BrU) is expected to provide valuable information on the mechanisms of damage of substituted and unsubstituted oligonucleotides.

In this communication, we report the low-energy (0.5−30 eV) ESD of neutral fragments, assigned to pyrimidine ring multibond dissociation, from different halogen-substituted Au/Cy*$_6$T$_3$ and Au/Cy*$_6$(FU,BrU,IU)$_3$ oligomers chemisorbed on

* Tél: 819-346−1110, ext. 14678. FAX: 819-564-5442. E-mail: lsanche@courrier.usherb.ca.

10.1021/jp9938112 CCC: $19.00
Published on Web 06/08/2000

an Au(111) substrate. From the analysis of the data, reaction pathways that lead to fragment desorption are suggested.

Sample Preparation and Experimental Method

HPLC-purified nonamers of fluoro-, bromo-, and iododeoxyuridine-substituted modified deoxycytidine (5′-Cy*(FU,BrU,IU)Cy*Cy*(FU,BrU,IU)Cy*Cy*(FU,BrU,IU)Cy*-3′) and a deoxythymidine analogue (5′-Cy*TCy*Cy*TCy*Cy*TCy*-3′) are chemisorbed onto a gold (111) surface. The gold surface is prepared by vacuum evaporation that has been shown to produce large terraces of crystalline Au(111) on mica.[28] The oligomers are anchored to the Au surface via a standard thioate modification at the phosphate moiety (P═S) on each of the six cytidine nucleotides (Cy*).[25] For the chemisorption procedure, a freshly deposited gold (111) substrate of about 20 cm^2 surface area is immersed into a solution of typically $\sim 3 \times 10^{15}$ molecules ($\sim$15−30 μL) of the dissolved oligo added to 50 mL of N_2-degassed Nanopure water, for 24 h. All oligonucleotides are bought from Keystone Labs and used without further purification.

The apparatus and the experimental method are described in detail elsewhere.[25] Eight Au/oligomer samples ($\sim$2 cm^2) are introduced into a load-lock chamber and are allowed to degas overnight at a pressure of approximately 1×10^{-6} Pa. The oligomers are free of the presence of a prominent hydration layer as verified by mass spectrometry; however, a minimal amount of structural water is likely to remain tightly bound to the oligonucleotides. The samples are afterward transferred into the analysis chamber, via a gate valve, where they are irradiated with low-energy electrons. The analysis chamber is equipped with a 1−200 amu residual gas analyzer (RGA) quadrupole mass spectrometer and a high-current (10^{-8}−10^{-5} A) custom-made electron gun, having an energy resolution of about 0.5 eV. By collimating the electron beam with an axial magnetic field, energies as low as 0.5 eV, which are limited by space charge and the finite energy resolution, can be reached.[29] The working background pressure in the analysis chamber is about 3×10^{-7} Pa. As we irradiate the thin oligomer films, the neutral particles (intact molecules or fragments) which desorb may enter the RGA where they are ionized and selected via their mass-to-charge ratios (m/z). The RGA monitors the amounts of the neutral gases present in the analysis chamber in terms of their relative partial pressures (RPPs). Experimentally, we record the time dependence of the RPP(t) of a specific m/z species, from background pressure, $RPP_{bk}(t)$ (i.e., with the electron beam off), to equilibrium pressure, $RPP_{sig}(t)$, resulting from electron irradiation during a short time ($\sim$8 s) at a fixed incident energy. The variation of RPP, ΔRPP, is obtained as $\langle RPP_{sig}\rangle - \langle RPP_{bk}\rangle$, where $\langle RPP_i\rangle = \sum RPP_i(t)\, dt)/\tau$, and τ represents an arbitrary time interval (<8 s). We repeat this procedure for the range of desired electron fluxes and electron energies. We further plot for each energy the number of fragments desorbed as a function of electron flux, which in all cases exhibits a linear relationship. We can then obtain, calculating the slope of the best linear-regression fit, the effective number of fragments desorbed per incident electron, at a specific electron energy. The details concerning the conversion from ΔRPP to a number of fragments desorbed (N_d) are given in ref 25. Briefly, at equilibrium, the number of fragments desorbed per unit time, $N_d/\Delta t$, is equal to the partial pressure variation, ΔRPP, times a factor of 1.3×10^{18} corresponding to SN/RT, where S is the true nominal pumping speed of the system, N is Avogadro's number, R is the perfect gas constant, and T is the temperature.

The effective number of a specific fragment desorbed per incident electron (N_d/N_e) is proportional to the effective desorption cross section (σ_{eff}) via

$$N_d/N_e \approx (N_0/a)\sigma_{eff} \qquad \text{(I)}$$

where N_0 is the initial number of target molecules in the irradiated area, a.[25] Because the chemisorbed oligonucleotides are anchored at six different positions, they are most likely to adsorb parallel to the surface. In this configuration, the impinging electrons strike an effective oligomer target essentially composed of nucleotide units facing the vacuum. The average number of *nucleotide units* N_0 is estimated to be 5.4×10^{13} in the irradiated area, a, of approximately 0.5 cm^2 (which is roughly constant over the entire range of electron energy),[29] when assuming that one flat-lying nonamer has a length of 4 nm and that the molecules are separated from each other by 2 nm, corresponding to standard parameters in double-stranded native DNA.[30] In a recent paper, Abdoul-Carime and co-workers chose to use a densely packed arrangement of oligomers adsorbed on Au(111) from which an upper limit of the average number of nucleotides per unit area was estimated.[26] Because we do not know the exact configuration adopted by these chemisorbed oligonucleotides on Au(111), both assumptions may be considered reasonable and, in any case, the estimated oligomer surface densities estimated do not vary largely (present, 1.2×10^{13} oligomers/cm^2; ref 26, 1.7×10^{13} oligomers/cm^2). Cross section comparison between the halodeoxypyrimidine-substituted oligonucleotides, and also with the thymine-substituted one, is based on the assumption that the oligomer surface coverage (i.e., the number of molecules per unit area) is, on the average, the same in all cases due to similar molecular structure and size. The error on σ_{eff} is principally attributed to uncertainties in N_d and N_0; however, the reproducibility of σ_{eff} lies within 25%, and its value is estimated to be reliable within a factor of 2. Finally, we note that the proximity of the gold substrate may reduce the yield of neutral fragment desorption. Indeed, it has been shown that the yield of H_2 produced experimentally from low-energy electron bombardment of methyl-terminated alkanethiol depends strongly on the length of the molecular chain studied, because the metal substrate tends to quench the dissociative attachment process.[31] This result suggests then that our measured yield would be larger if recorded in more biological environments.

Results

The present low-energy (0.5−30 eV) electron irradiation on thymine- and halogen-substituted chemisorbed nonamers [i.e., $Au/Cy^*_6(T \text{ or FU, BrU, IU})_3$] yields two major neutral fragments of mass-to-charge (m/z) ratios of 26 and 42, assigned respectively to CN and OCN. Figure 1 presents the CN and OCN effective desorption cross sections (σ_{eff}) for the various chemisorbed oligomers calculated from eq I using the N_d/N_e values measured between 0.5 and 30 eV incident energy. It shows that, basically, all of the neutral fragment desorption cross sections exhibit a similar shape as a function of electron energy, with the exception of a very low energy feature in the yield function of the BrU-oligo, shown on an extended energy scale in Figure 2. The CN σ_{eff} dependence between 0.5 and 5 eV (not shown for clarity) is essentially similar in shape and intensity to that obtained for OCN. With the exception of the result for the BrU-oligo, the desorption yields are barely discernible from the background noise below 4 eV. For all cross-section curves in Figure 1, a threshold appears near 5−6 eV, as shown more clearly in Figure 3. Above the energy of that threshold, the cross sections sharply rise to about 12−13 eV. In Figure 3, the CN

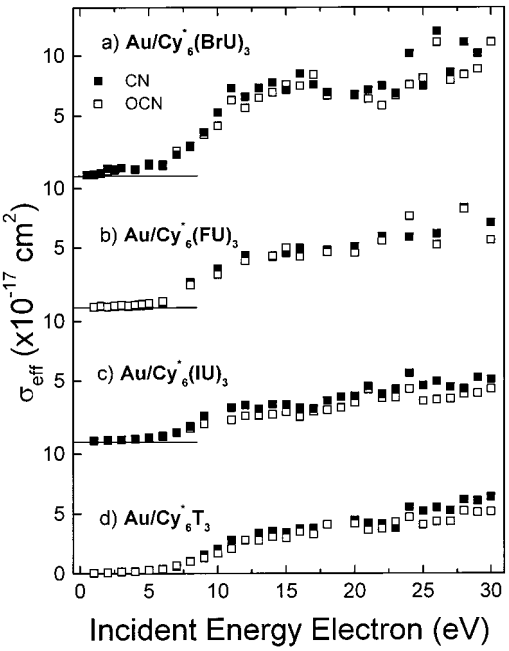

Figure 1. Effective cross sections σ_{eff} for the desorption of CN (■) and OCN (□) induced by 0.5−30 eV electron impact on (a) $Cy^*_6(BrU)_3$, (b) $Cy^*_6(FU)_3$, (c) $Cy^*_6(IU)_3$, and (d) $Cy^*_6(T)_3$ oligomers chemisorbed on a gold substrate. Error bars are omitted for clarity, but typically the relative error does not exceed about 25% of the measured values. Each data point is the average of at least three distinct experiments.

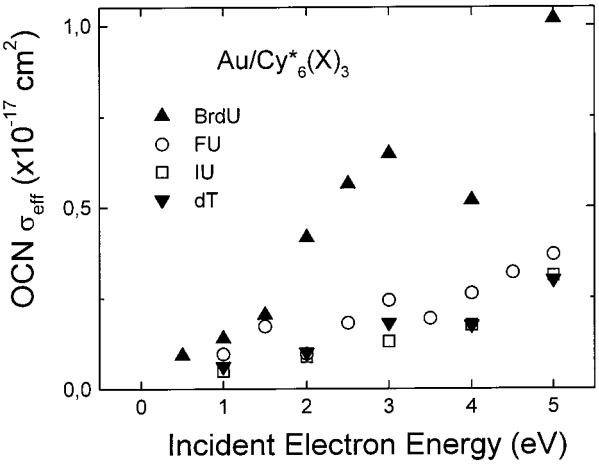

Figure 2. OCN effective desorption cross sections measured between 0.5 and 5 eV for the various substituted oligomers of deoxycytidine phosphate: BrU (▲), FU (○), IU (□), and T (▼). The CN desorption data are not shown but they are similar to those for OCN. Error bars are omitted for clarity, but typically the relative error does not exceed about 25% of the measured values. Each data point is the average of at least three distinct experiments.

cross sections are omitted for clarity of the graph, but, referring to Figure 1, one can observe that they are essentially identical to the OCN cross sections. Between ~12 and 20 eV, the cross sections show a moderate increase or broad peak, followed by a monotonic rise up to 30 eV. On the average, the cross sections decrease in the order BrU > FU > IU ≈ T. However, within each oligomer investigated, the CN/OCN desorption cross-section ratio is constant over the entire energy regime. No halogen-containing fragments were observed to desorb from the halogen-substituted oligonucleotides. No entire DNA base, nucleoside, or nucleotide was detected either; if these latter high molecular mass (>100 amu) species are indeed created during

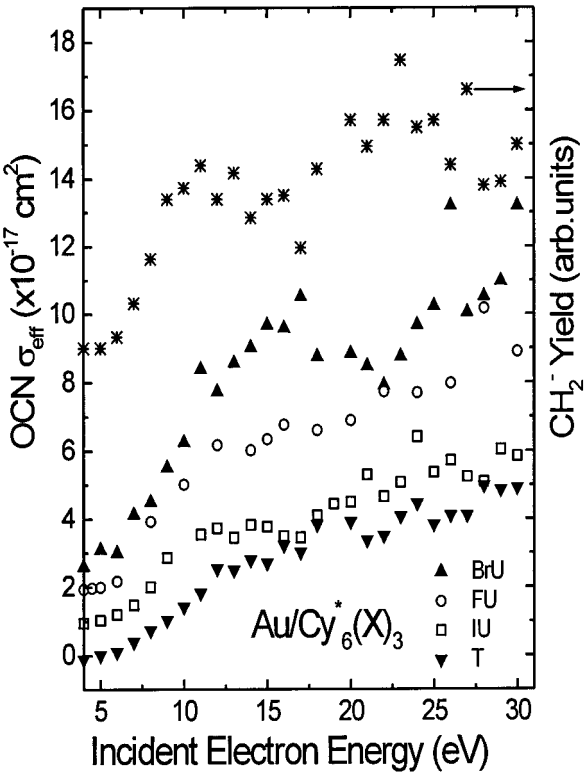

Figure 3. The curve on top (*) represents the incident electron energy dependence of CH_2^- yield produced via low-energy electron bombardment of a thin film of thymine (ref 24). The other curves are the OCN effective desorption cross sections between 5 and 30 eV for the various substituted oligomers of deoxycytidine phosphate: BrU (▲), FU (○, IU (□), and T (▼). The CN desorption data are not shown but they are similar to those for OCN. Error bars are omitted, but each data point is the average of at least three distinct experiments that do not vary by more than 25%. The curves are displaced vertically for clarity.

irradiation, they are not expected to significantly desorb from the thin films. A priori, the signal at mass 42 could also arise from the production of H_2NCN. However, because this fragment cannot emerge from the thymine and halouracil bases, its production cannot account for the change in the cross sections observed in Figures 1−3, upon substitution of a methyl group by a fluorine, bromine, or iodine atom on the uracil ring. We therefore limit the following discussion to CN and OCN production. In previous work, we showed that the detected CN is not predominantly related to cracking of OCN^+ into the RGA.[25]

Discussion

Primary Electron−Molecule Interaction and Subsequent Decay Channels. We present first the possible ultrafast events following the primary electron−molecule interaction. Figure 4 describes the immediate reaction pathways of a low-energy electron with a hypothetical AB molecule.[10] The electron interaction may produce an excited neutral state of the molecule (AB*) via pathway a. AB* may dissipate its excess energy via photon emisson and/or energy transfer to the surrounding medium, a. If the configuration of the excited state is dissociative, AB* may dissociate into two neutral radicals, as proposed by the a2 pathway. Above a certain energy threshold (~14−16 eV) fragmentation via dipolar dissociation (DD), path a3, yields an anion and a cation. The incident electron may also temporarily attach to the molecule via the b pathway and then autoionize via path b2 or, for a sufficiently long-lived anion in a dissociative state, it may fragment into a stable anion and a

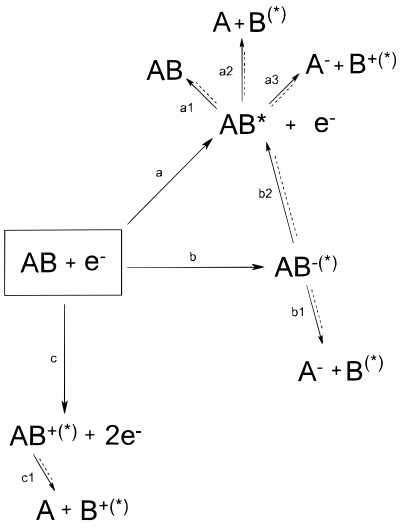

Figure 4. Immediate reaction pathways following electron interaction with a diatomic molecule AB.

neutral atom or radical, b1; this latter mechanism is known as DEA. When the AB^- state lies above the energy of the first electronically excited state of AB, AB* can be electronically excited after electron autodetachment b2; in this case, it could decay into the a1, a2, and a3 pathways previously described. Finally, the incoming electron can directly ionize the molecule via path c, and if the resulting cation is dissociative, it may fragment, as schematically shown by reaction c1.

Resonant and Nonresonant Initial Dissociative Processes in the DNA Bases. Because the detected fragments arise from the low-energy electron interaction with the base residues in the oligomer structure, we now discuss the possible dissociation processes in the DNA bases. We first note that the prominent peak seen in Figure 2 for the BrU-oligo is indicative of a resonant process. Thus, this well-defined feature, starting between 1 and 2 eV and peaking at 3 eV, reveals the occurrence of pathway b in Figure 4. In other words, it indicates CN and OCN production initiated via DEA. Furthermore, because the thresholds for electronic excitations of the DNA bases in the solid-phase lie near 5−6 eV,[32] *formation of a* BrU^- *shape resonance, followed by its dissociation into* Br^- *and U (path* b1 *in Figure 4), is the only fragmentation mechanism possible at such low energies.*[10] It has been demonstrated that near-thermal electrons resonantly react with BrU, BrdU (bromodeoxyuridine), and BrdUMP (bromodeoxyuridine monophosphate) to form the ground-state stable bromide ion and the associated radicals.[33,34] DEA has also been directly observed at higher energies in the ESD of Br^- from BrU thin films.[24] The Br^- desorption yield function exhibits a threshold at 3 eV and a peak at 6 eV. Furthermore, the Br^- detected by XPS in BrU films that had been bombarded with soft X-rays [35] and low-energy electrons was attributed to resonant 0−5 eV electron capture.[24] Thus, the experimental data shown in Figure 2 indicate that the specific resonant cleavage of the C−Br bond, yielding the concomitant reactive uracil radical (U), is responsible for the CN and OCN formation below 5 eV.

Between 5 and 15 eV incident energy, path a becomes accessible. The electronically excited neutral DNA base (5-XU*) may decay via a2 to produce two neutrals, such as X + U•. Along with nonresonant processes, temporary electron capture via the formation of a core-excited resonance and subsequent dissociation of the transient molecular anion is also possible above 5 eV. ESD of F^-, Br^-, I^-, and CH_2^- from FU, BrU, IU, and T solids, respectively, attributed to DEA are indeed observed above 5 eV incident electron energy.[24] As an illustration, the top curve in Figure 3 displays the incident electron-energy dependence of the latter anion yield produced via low-energy electron impact on a five-monolayer film of thymine. In addition, desorptions of H^- (peak at 8−9 eV) and O^- (broad peak between 12 and 15 eV) are also measured from such thin films.[24] These recent anion ESD results suggest the concomitant production of the following radical counterparts via pathway b→b1:

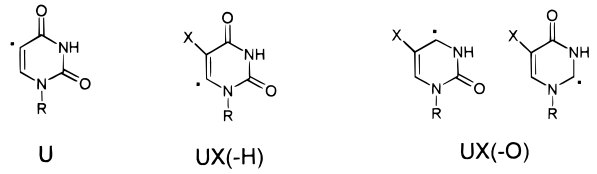

A priori, these radicals can also be formed via pathways a→a2 and b→b2→a2.

The well-known uracil radical U• is formed via rupture at the 5 position. The UX(−H) radical is the result of H^- (H) abstraction at position C(6), and the UX(−O) radical is created after the O^- (O) production at position C(2) or C(4) from electron-irradiated T, FU, BrU, and IU solids. We propose the occurrence of similar electron−DNA base reactions with the bases in the oligomer structure, accompanied by the formation of the various U, UX(−H), and UX(−O) reactive radicals, which may further react to yield the observed neutral fragments. The prominent ∼15 eV broad peak appearing in the BrU-oligo cross sections is indicative of a high-energy resonant reaction, most likely caused by the initial formation of a core-excited resonance as proposed by Abdoul-Carime et al.[26] High-energy DEA processes in BrU have been observed through CN^- (14 eV), OCN^- (13−14 eV), and O^- (12−13 eV) desorption from BrU thin films,[24] suggesting that similar DEA processes may also occur with the BrU residue in the oligomer.

As we demonstrated, the desorption cross sections at low-impact energies depend on the chemical nature of the C(5) substitute, with the U radical as the only reactive species formed below 5 eV. On the other hand, above 5 eV, *the similarity of shape between the cross-section curves presented in Figure 3 suggests that CN and OCN production reactions are equivalent for all DNA bases investigated*. Because C(6)−H and C(2,4)═O are functional groups common to the four T, FU, BrU, and IU residues, the UX(−H) and UX(−O) radicals, originating from resonant and nonresonant cleavages of the latter intramolecular bonds, are likely to be involved, along with U, in neutral fragment production above 5 eV. Above ∼15 eV, we do expect some contribution of the positive species formed via DD a3 (e.g., $H^- + [UX(-H)]^+$) and ionization c processes.

Proposed Mechanisms for the Neutral CN and OCN Formation/Desorption. Because the nitrogen-containing CN and OCN neutral species must originate from the aromatic ring of the DNA base, we now focus on the fate of the electron-induced U, UX(−H), and UX(−O) reactive radicals. Reaction of the base radicals with adjacent DNA components, which may proceed via various competing channels such as hydrogen abstraction, dimerization, or cross-linking,[36] is not likely to be responsible for the observed pyrimidine-ring neutral fragments production. Dimerization and cross linking lead to formation of larger molecular adducts, while hydrogen abstraction generates a base or sugar radical. Moreover, these reactions are expected to be significantly reduced due to the restricted mobility of the radicals within the oligo structure and the absence of a suitable H atom donor in such a solid system.

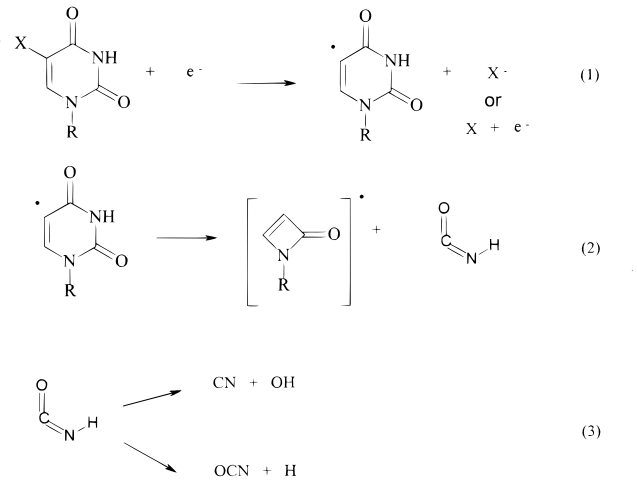

Figure 5. Proposed reactions leading to the formation/desorption of CN and OCN neutral fragments via the uracil radical (U) production from XU as an initial step (X = CH_3, F, Br, or I).

Therefore, attack of the primary radical on adjacent residues is not considered a major process leading to CN and OCN formation.

The common feature in each of the U, UX(−H), and UX(−O) primary radicals created via electron interaction is the presence of an isocyanic acid (OCNH) moiety within their molecular structure. *We therefore propose that extrusion of an unstable OCNH moiety and its subsequent dissociation are responsible for CN and OCN formation/desorption*. This is, furthermore, consistent with our observation of a constant CN/OCN ratio over the entire energy range studied (see Figure 1), suggesting their production from a single intermediate source, viz., the OCNH radical. The force driving U, UX(−H), and UX(−O) toward unimolecular fragmentation is principally the instability of the σ-orbital-localized radical,[37] coupled with the excess internal energy transferred into the ring via electron interaction. As pointed out earlier, the restricted mobility imposed by the chemical adsorption and the absence of suitable H-atom donors are additional causes leading to radical unimolecular dissociation instead of attack.

At this point, we have established the most probable first and last steps of the CN and OCN formation/desorption mechanisms. The first step is the electron-induced resonant and nonresonant U, UX(−H), or UX(−O) reactive radical formation (e.g., reaction 1 in Figure 5). The final step is the production of CN and OCN from the unstable OCNH moiety via thermodynamically favored dissociations (reaction 3 in Figure 5). In support of this latter assumption, Abdoul-Carime and co-workers recently demonstrated that CN and OCN detected from electron bombardment of thymine- and bromouracil-substituted oligonucleotides are not formed by the isocyanic acid cation cracking into the mass spectrometer.[26]

Neither the present experiment nor the literature data were able to provide indications to elucidate the intermediate step(s) between reaction 1 in Figure 5 and OCNH dissociation. In the case of U radical unimolecular dissociation, we tentatively propose that a ring-opening reaction leads to extrusion of the OCNH moiety, possibly via cyclization to a β-lactam-like product. We show in Figure 5 the proposed U-radical-mediated CN and OCN production reaction. Although we did not attempt to draw a similar picture of the steps leading to CN and OCN from UX(−H) and UX(−O), ring-opening reactions are also likely to be involved in these cases. *The linear relationship observed for the CN and OCN desorption yields as a function of electron flux indicates a single-electron process, consistent with the proposed pathway*.

The reaction scheme in Figure 5 is further supported by threshold energy calculations based on average bond energies and electron affinities.[38,39] Calculated formation thresholds, along with experimental desorption thresholds and effective desorption cross sections measured at 3 and 15 eV, are reported in Table 1. We find good agreement between the calculated formation energies (∼1.5 eV) and the experimental desorption thresholds (1−2 eV) of CN and OCN via the Br^- + U DEA process. There is a poorer threshold correlation for the resonant halide-mediated CN and OCN formation mechanism in the case of the FU- and IU-oligomers. All 5−6 eV desorption thresholds are consistent with both nonresonant rupture at C(5)−X and resonant bond cleavage at C(6)−H that should exhibit thresholds between 4.5 and 6.5 eV, and near 5.5 eV, respectively.

Effect of the DEA Dynamics and Dissociation Channel on the Neutral Fragments Desorption Cross Sections. Below 5 eV, the neutral fragment cross sections depend on the C(5)−X DEA cleavage of the XU residues via pathway b→b1 shown in Figure 4. In this section, we show that the dynamics of the DEA process may be responsible for the relative magnitude of the observed CN and OCN yields of the different T- and halogen-substituted oligomers. To estimate the relative amplitude of the U-radical yields, the released X^- kinetic energy in the dissociation of XU and the transient $(XU)^-$ survival probability are calculated using O'Malley's theory of DEA.[40] The kinetic energy indicates whether $(XU)^-$ dissociation is energetically allowed, whereas the survival probability reflects the magnitude of the process. The solid line in Figure 6 represents the potential energy of ground-state XU along the X−U coordinate, for X = CH_3, F, Br, and/or I, while the different dash curves represent the hypothetical potential energy curves for XU^- (X = F, Br, and/or I) along the same coordinate. These latter curves are considered to be purely repulsive so that they can lead to DEA. Assuming that the dissociation occurs in the ground state, the initial kinetic energy of the X^- fragment may be expressed as $E_K(X^-) = (M_U/[M_U + M_X])(EA(X) - D(X-U) + \epsilon)$,[41] where M_U and M_X represent the molecular mass of each fragment and ϵ is the incident electron energy, EA(X) is the electron affinity of the fragment X, and D(X−U) is the dissociation energy for the X−U bond of the neutral molecule. In addition to kinetic energy considerations, the survival probability of the XU^- ion is an important parameter in dissociation because the anion lifetime must be long enough to allow sufficient separation between X^- and U within the anion before electron autodetachment in order to stabilize the excess electron on fragment X. The probability for $(X-U)^-$ to successfully dissociate may be approximated by $P_S \approx \exp -(\iota_d/\iota_a)$, where ι_a represents the electron autodetachment lifetime (taken here as a typical anion lifetime of 2×10^{-14} s) and ι_d is the dissociation lifetime (i.e., the time beyond which autoionization is no longer possible and separation occurs with the extra electron bound to fragment X). In that case, the transient anion survives after the crossing point $R_{(C \text{ or } C')}$ in Figure 6. According to the Franck−Condon (FC) principle, for any appreciable X^- production, ι_d must be a sizable fraction of the period T_{C-X}, corresponding to one X−U vibration in the neutral state (see Figure 6). We therefore, as a first approximation, take one-eighth of that value for the calculation of the survival probabilities of the X^- anions. The various kinetic energies and survival probabilities are listed in Table 2 for ϵ = 3 eV, along with other parameters relevant to the calculations.

Dissociation into the limit U + CH_3^- (or U + H + CH_2^-) is forbidden at and below 3 eV as shown, for instance, by the

TABLE 1: Empirical (Formation) and Experimental (Desorption) Thresholds for the Resonant (+) and Nonresonant CN and OCN Production from Au/Cy*$_6$(X)$_3$ (where X = FU, BrU, IU, and T) Chemisorbed Oligomers, via the Proposed Uracil-like Radical-Mediated Mechanisms in Figure 5[a,b]

DNA base residue	formation thresholds via abstraction at the 5 position (eV)	formation thresholds via abstraction at the 6 position (eV)	experimental thresholds (eV)	σ_{eff} (3 eV) ($\times 10^{-17}$ cm^2)	σ_{eff} (15 eV) ($\times 10^{-17}$ cm^2)
BrU	1.6$^+$ (CN)	5.5$^+$ (CN)	1−2	0.6−0.7	∼7.5
	1.7$^+$ (OCN)	5.6$^+$ (OCN)			
	4.9 (CN)	6.3 (CN)	5−6		
	5.0 (OCN)	6.4 (OCN)			
FU	3.1$^+$ (CN)	5.5$^+$ (CN)	5−6	∼0.2	∼4.5
	3.2$^+$ (OCN)	5.6$^+$ (OCN)			
	4.9 (CN)	6.3 (CN)			
	5.0 (OCN)	6.4 (OCN)			
IU	1.4$^+$ (CN)	5.5$^+$ (CN)	5−6	∼0.2	2.5−3
	1.5$^+$ (OCN)	5.6$^+$ (OCN)			
	4.5 (CN)	6.3 (CN)			
	4.6 (OCN)	6.4 (OCN)			
T	4.4$^+$ (CN)	5.5$^+$ (CN)	5−6	∼0.2	3−3.5
	4.5$^+$ (OCN)	5.6$^+$ (OCN)			
	5.5 (CN)	6.3 (CN)			
	5.6 (OCN)	6.4 (OCN)			

[a] The effective CN and OCN desorption cross sections at 3 and 15 eV are also included. [b]Empirical threshold calculations are based on values found in ref 38 and 39.

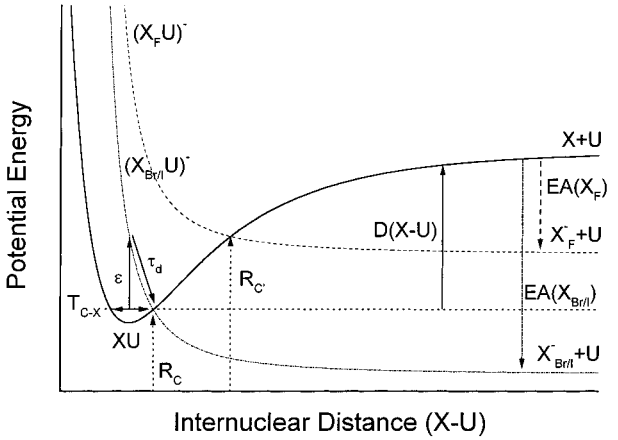

Figure 6. Schematic representation of the potential energy curves of neutral substituted uracil, XU (solid line), and its anion XU$^-$ (dashed lines) along the X−U internuclear coordinate, where X can be CH_3, F, Br, or I, and U is the uracil aromatic ring radical. The latter curves, which can lead to DEA, are chosen to be purely repulsive potential energy. $R_{(C\ or\ C')}$ represents the crossing point beyond which electron autodetachment can no longer occur; T_{C-X} is a vibrational period of the neutral molecule, while τ_d (which is a fraction of T_{C-X}) defines the dissociation lifetime (see text). ϵ stands for the incident electron energy. The energy difference between the asymptote of the neutral and the anionic potential curves corresponds to the electronic affinity EA(X) of the fragment X, while the dissociation energy for the X−U bond, D(X−U), is given by the difference between the lowest vibrational state and the asymptote of the neutral potential curve.

negative kinetic energy value obtained for the methyl anion (−0.38 eV), which is consistent with the observation of the anion production induced by low-energy electron impact on DNA bases in either gas-[42] or condensed-phase[24] experiments. Indeed, in those works, no methyl anions were observed below 6 eV incident electron energy, while above this energy resonant production of CH_2^- is detected. At 3 eV, where dissociation of halides is energetically allowed, the survival probability of the transients gives the ratios $P_S(FU^-)/P_S(BrU^-) \approx 17$ and $P_S(BrU^-)/P_S(IU^-) \approx 5$, clearly indicating that a larger signal is expected via DEA from the BrU$^-$ anion than from the IU$^-$ anion. Transient BrU$^-$ and IU$^-$ probably have similar potential energy curves as assumed in Figure 6; so it seems that the differences in observed yields may depend simply on the ability

TABLE 2: X$^-$ Kinetic Energies (E_K), Calculated at 3 eV Incident Energy, along with the Survival Probabilities (P_S) of the (XU)$^-$ Transient Ion[a]

X$^-$	M (amu)	EA(X)[b] (eV)	D_{C-X}[c] (eV)	E_K(X$^-$) formed at 3 eV (eV)	ι_d (10^{-14} s)	P_S(XU$^-$)
CH_3^-	15	0.08	3.51	−0.38	3.1	2.1×10^{-1}
F$^-$	19	3.45	4.55	1.62	2.8	2.5×10^{-1}
Br$^-$	80	3.36	2.91	2.00	8.4	1.5×10^{-2}
I$^-$	127	3.06	2.47	1.67	11.4	3.3×10^{-3}

[a] We also list in this table the molecular mass (M) of the fragments, the electron affinity (EA), the carbon−X average bond energy (D_{C-X}), and the dissociation lifetime ι_d estimated as one-eighth of the ground-state DNA base C−X vibration period. [b] Reference 39. [c] Reference 38.

of Br$^-$ to dissociate faster that I$^-$ due to its lighter mass. As seen from the values in Table 2, such an explanation is not valid to account for the low yields observed from the fluorinated oligomer below 5 eV. However, comparison between known potential energy curves of simpler organic halides (e.g., CH_3F, CH_3Br, and CH_3I)[43] indicates a general trend for the fluorinated anion to lie at higher energy, as drawn in Figure 6. This difference may completely modify the probability to form the initial transient anion (e.g., the electron capture cross section) below 5 eV. As shown in Figure 6, the FC transition at incident energies below 5 eV is less favorable for FU than for BrU and IU. Thus, within the 0.5−5 eV regime, the combination of survival and electron-capture probabilities gives a firm argument to explain the magnitude BrU > FU and BrU > IU for the cross sections seen in Figure 2. On the other hand, above 5 eV, along with U radical formation, we propose involvement of UX(−H) and UX(−O) reactive species. As calculated and reported in Table 1, CN and OCN production from unimolecular fragmentation of the UX(−H) radicals possesses thresholds near 5.5 eV. The latter are expected to lie at higher energies from the UX(−O) radicals because of the larger energy required to break the carbonyl bond. Therefore, above 5 eV, the cross sections arising from UX(−H) and UX(−O) fragmentation are superimposed on variable yields originating from the U radical. In other words, the cross-section intensity variations between the irradiated oligomers most likely depend on the *number* of accessible C(5)−X dissociative channels.

Within each of the oligomers investigated, the energy dependence of desorption cross sections is practically identical for the CN and OCN; moreover, their ratio is near one and constant throughout the energy range (see Figure 1). This observation leads to two considerations: (a) both neutral fragments are likely to come from the same electron-induced intermediate, which is consistent with the proposed mechanisms, and (b) the scission probability of the unstable OCNH moiety is equal for both dissociation channels, which is in part supported by our calculated empiric CN and OCN formation thresholds. However, this observation is slightly different from the results obtained in a previous work on low-energy electron irradiation of homooligomers, which shows that the CN desorption cross sections are larger than those of OCN for incident energies over 10 eV.[25] The latter observations suggest that a change in the chemical environment within the oligomer may modify the branching ratios for the CN and OCN formation from the unstable OCNH intermediate, or it may indicate that homogeneous base sequences (such as satellite portions of DNA) show a different sensitivity to >10 eV electron attack compared to heterogeneous sequences.

Pyrimidine Ring Fragmentation and Cellular Radiosensitization. It has been proposed that enhancement of radiation damage upon incorporation of halodeoxyuridines (more specifically BrdU) in cellular DNA is due to an ~0 eV DEA-mediated mechanism.[36,44,45] However, pyrimidine ring fragmentation is not observed near 0 eV in the present experiment. The U radical created by interaction of a near 0 eV electron in our experiment either stays unreacted facing vacuum or results in damage that we are unable to probe (e.g., dimer formation). In any case, CN and OCN desorption from fragmentation of the U radical cannot occur at such low energy because there is not sufficient internal energy available for this process near 0 eV (see Table 1).

The present experimental results are consistent with the generally observed larger electron-induced damage efficacy for the BrU residue among the 5-halouracils. *The BrU vs T enhancement is observed over most of the energy regime, suggesting that bromouracil radiosensitization[36,44,45] is due not only to the solvated electrons but also to higher energy electron interactions before their thermalization.* Thus, the larger production of resonant (and also direct-scattering) 0.5−30 eV electron-induced radicals, specifically U, is proposed to be in a large part responsible for the observed BrU-mediated radiosensitization. The FU-mediated sensitization, roughly 1.5 times more than that of T, is also likely to be related to the amount of primary reactive radical produced. Although they do not incorporate into the DNA structure, the radicals derived from electron interaction with FU residues *nearby* DNA may be harmful. In the case of the IU-oligomer, it appears that its radiosensitization mechanisms are more likely related to higher energy (>30 eV) interactions, resulting in Auger electron cascades, for example.[44]

Finally, we note that the oligonucleotides studied in the present experiment are not paired, as they would be in DNA. Thus, we can expect that these single strands are more susceptible to low-energy electron damage via base dissociation, because the bases are facing the electron beam incoming from vacuum. In that respect, the present studies may be more specifically related to low-energy electron attack on the bases during cell division when the DNA strands separate. We are planning to study short chemisorbed double DNA strands to shed more light on this question. In any case, it is now known that 3−20 eV electrons can cause single- and double- strand breaks in DNA by dissociative electron attachment induced reactions.[46]

Summary

We have shown that the impact of electrons (of energies below 30 eV) on Cy^*_6(T and FU, BrU, $IU)_3$ oligomers chemisorbed on gold produces ring fragmentation of the DNA bases leading to the formation and desorption of CN and OCN (H_2NCN) neutral fragments. The 5−30 eV fragmentation is principally initiated via transitory electron capture by the bases and direct inelastic scattering which can result in the formation of U, UX(−H), and UX(−O) DNA base radicals. We propose that the radicals undergo unimolecular dissociation leading to the extrusion of an unstable OCNH moiety, which further dissociates to yield the observed CN and OCN. Unimolecular fragmentation of the U radical initiated via DEA is the *only* CN and OCN production pathway below 5 eV. Simple energetic calculations provide good qualitative arguments to explain this result. Above ~15 eV, fragmentation of positive radicals formed via DD may also take place. The constant ratio of the CN and OCN yields observed over the entire energy regime for all oligomers irradiated is indicative of the occurrence of a single source leading to the neutral fragment desorption, i.e., the OCNH moiety.

Over most of the energy range, the magnitude of desorption cross sections as a function of the substituted residue follows the sequence BrU > FU > IU ≈ T, where the difference between BrU and T is about 2- to 3-fold. As demonstrated in the majority of radiosensitization-oriented works, the BrU substitute appears to be the most sensitive to electron interaction among the 5-halouracils. The results also suggest that halodeoxypyrimidine-mediated radiosensitization is due not only to solvated electrons but also to events that occur before electron thermalization.

Acknowledgment. This study is sponsored by the Medical Research Council (MRC) and the National Cancer Institute of Canada. Thanks are extended to Drs. Dean Antic, Andrew D. Bass, Marc Michaud, and Anthony J. Waker, and Profs. Michael A. Huels and Michael D. Sevilla for very fruitful discussions and enlightening comments.

References and Notes

(1) Ramsier, R. D.; Yates, J. T., Jr. *Surf. Sci. Rep*. **1991**, *12*, 247 and citations therein.
(2) Stulen, R. H., Knotek, M. L., Eds. *Desorption Induced by Electronic Transition DIET III: Proceedings of the Third International Workshop*; Springer Series in Surface Sciences 13; Springler-Verlag: Berlin, 1988.
(3) Harris, T. D.; Lee, D. H.; Blumberg, M. Q.; Arumainayagam, C. R. *J. Phys. Chem*. **1995**, *99*, 9530.
(4) Xu, C.; Koel, B. E. *Surf. Sci.* **1993**, *292*, L803.
(5) Donnelly, V. M.; Herman, I. P.; Hurose, M. *Photon, Beam and Plasma Simulated Chemical Processes at Surfaces*; Mater. Res. Soc. Symp. Proc.; Material Research Society: Pittsburgh, PA, 1987.
(6) Matsui, S.; Mori, K. *Jpn. J. Appl. Sci.* **1984**, *23*, L706.
(7) Corcoran, E. *Sci. Am.* **1990**, *263*, 98.
(8) Lacombe, S.; Cemic, F.; Jacobi, K.; Hedhili, M. N.; LeCoat, Y.; Azria, R.; Tronc, M. *Phys. Rev. Lett.* **1997**, *79*, 1146.
(9) Alberas-Sloan, D. J.; White, J. M. *Surf. Sci.* **1996**, *365*, 212 and citations therein.
(10) Sanche, L. *Scanning Microsc.* **1995**, *9*, 619.
(11) Sanche, L.; Parenteau, L. *Phys. Rev. Lett.* **1987**, *59*, 136.
(12) Kimmel, G. A.; Orlando, T.; Cloutier, P.; Sanche, L. *J. Phys. Chem. B* **1997**, *101*, 6301.
(13) Rowntree, P.; Dugal, P. C.; Hunting, D.; Sanche, L. *J. Phys. Chem.* **1996**, *100*, 4546.
(14) For a review see: Bass, A. D.; Sanche, L. *Radiat. Environ. Biophys.* **1998**, *37*, 243.
(15) Di, W.; Rowntree, P.; Sanche, L. *Phys. Rev. B* **1995**, *52*, 16618. Olsen, C.; Rowntree, P. A. *J. Chem. Phys.* **1998**, *108*, 3750.

(16) Avouris, P. *J. Phys. Chem*. **1990**, *94*, 2246.
(17) Quate, C. F. *Surf. Sci.* **1997**, *386*, 259.
(18) Dai, H.-L., Ho, W., Eds. *Laser Spectroscopy and Photochemistry on Metal Surfaces*; World Scientific: Singapore, 1995.
(19) Sanche, L. *IEEE Trans. on Dielectr. Electr. Insul.* **1997**, *4*, 507.
(20) Sieger, M. T.; Simpson, W. C.; Orlando, T. M. *Nature* **1998**, *394*, 554.
(21) Johnson, R. E. *Energetic Charged-Particle Interactions with Atmospheres and Surfaces*; Physics and Chemistry in Space Planetology; Springer-Verlag: Berlin, 1990; Vol. 19.
(22) Sanche, L. *J. Chim. Phys.* **1997**, *94*, 216.
(23) Cobut, V.; Frongillot, Y.; Patau, J.-P.; Goulet, T.; Fraser, M.-J.; Jay-Gerin, J.-P. *Radiat. Phys. Chem*. **1998**, *51*, 229.
(24) Herve du Penhoat, M.-A.; Huels, M. A.; Cloutier, P.; Jay-Gerin, J.-P.; Sanche, L. *Abstracts of the Eleventh International Congress of Radiation Research*, Dublin, Ireland, 1999. Article to be submitted for publication.
(25) Dugal, P.-C.; Huels, M. A.; Sanche, L. *Radiat. Res.* **1999**, *151*, 325.
(26) Abdoul-Carime, H.; Dugal, P.-C.; Sanche, L. *Radiat. Res.*, **2000**, *153*, 23.
(27) Rabke-Clemmer, C. E.; Leavitt, A. J.; Beebe, T. P., Jr. *Langmuir* **1994**, *10*, 1796.
(28) Kang, J.; Rowntree, P. A. *Langmuir* **1996**, *12*, 2813.
(29) Leclerc, G.; Zuolin, C.; Sanche, L. *J. Phys. Chem*. **1987**, *91*, 6461.
(30) Reithel, F. J. *Concepts in Biochemistry*; McGraw-Hill: New York, 1969; Chapter 18.
(31) Rowntree, P.; Dugal, P. C.; Hunting, D.; Sanche L. *J. Phys. Chem*. **1996**, *100*, 4546.
(32) Crewe, A. V.; Isaacson, M.; Johnson, D. *Nature* **1971**, *231*, 262.
(33) Zimbrick, J. D.; Ward, J. F.; Myers, L. S. *Int. J. Radiat. Biol.* **1969**, *16*, 505.
(34) Ye, M. Y.; Shen, Y. *J. Liq. Chromatogr*. **1994**, *17*, 773−791.
(35) Klyachko, D. V.; Huels, M. A.; Sanche, L. *Radiat. Res.* **1999**, *151*, 177.
(36) Wang, W.; Razskazovskii, Y.; Sevilla, M. D. *Int. J. Radiat. Biol.* **1997**, *71*, 387.
(37) Streitwieser, A., Jr.; Heathcock, C. H. *Introduction to Organic Chemistry*, 3rd ed.; Macmillan Publishing: New York, 1985.
(38) Lowry, T. H.; Richardson, K. S. *Mechanism and Theory in Organic Chemistry*, 3rd ed.; Harper Collins: New York, 1987; Chapter 2, Thermochemistry.
(39) *CRC Handbook of Chemistry and Physics*, 65th ed.; CRC Press: Boca Raton, FL, 1984.
(40) O'Malley, T. F. *Phys. Rev.* **1966**, *150*, 14.
(41) Christophorou, L. G. *Atomic and Molecular Radiation Physics*; Wiley-Interscience: New York, 1971; Chapter 6, Negative Ions.
(42) Huels, M. A.; Hahndorf, I.; Illenberger, E.; Sanche, L. *J. Chem. Phys.* **1998**, *108*, 1309.
(43) Krzysztofowicz, A. M.; Szmytkowski, C. *J. Phys. B: At., Mol. Opt. Phys.* **1995**, *28*, 1593.
(44) Iliakis, G.; Pantelias, G.; Kurtzman, S. *Radiat. Res.* **1989**, *119*, 286.
(45) Larson, D.; Bodell, W. J.; Ling, C.; Phillips, T. L.; Schell, M.; Schrieve, D.; Troxel, T. *Int. J. Radiat. Biol.* **1989**, *16*, 171.
(46) Boudaiffa, B.; Cloutier, P.; Hunting, D.; Huels, M. A.; Sanche, L. *Science*, **2000**, *287*, 1658.